Available online at www.sciencedirect.com

ScienceDirect

Transactions of A. Razmadze Mathematical Institute 170 (2016) 243–265

Transactions of A. Razmadze Mathematical Institute

www.elsevier.com/locate/trmi

Original article

Thermal diffusion and diffusion thermo effects on unsteady MHD fluid flow past a moving vertical plate embedded in porous medium in the presence of Hall current and rotating system

G. Jithender Reddy[a,*], R. Srinivasa Raju[b], P. Manideep[c], J. Anand Rao[d]

[a] *Department of Mathematics, VNR Vignana Jyothi Institute of Engineering and Technology, Hyderabad, Ranga Reddy(Dt), 500090, Telangana State, India*

[b] *Department of Mathematics, GITAM University, Hyderabad Campus, Rudraram, Medak (Dt), 502329, Telangana State, India*

[c] *Department of Mathematics, Sphoorthy Engineering College, Nadargul, Saroornagar, Ranga Reddy(Dt), 501510, Telangana State, India*

[d] *Department of Mathematics, Faculty of Science, Osmania University, Hyderabad, 500007, Telangana State, India*

Received 19 May 2016; received in revised form 15 June 2016; accepted 1 July 2016

Available online 25 July 2016

Abstract

In this research paper, numerical study of unsteady magnetohydrodynamic natural convective heat and mass transfer of a viscous, rotating fluid, electrically conducting and incompressible fluid flow past an impulsively moving vertical plate embedded in porous medium in the presence of ramped temperature, thermal radiation, hall current, thermal diffusion and diffusion thermo is investigated. The fundamental governing dimensionless coupled boundary layer partial differential equations are solved by an efficient Element Free Galerkin Method (EFGM). Computations were performed for a wide range of some important governing flow parameters viz., Hall current, rotation, thermal diffusion (Soret) and diffusion thermo (Dufour). The effects of these flow parameters on primary and secondary velocity, temperature and concentration fields for externally heating and cooling of the plate are shown graphically. Finally, the effects of these flow parameters on the rate of heat, mass transfer and shear stress coefficients at the wall are prepared through tabular forms for heating and cooling of the plate. Also, these are all discussed for ramped temperature and isothermal plates. We have shown that some results are in good agreement with earlier reported studies.

Keywords: Heat transfer; MHD; Hall current; Rotation; Element Free Galerkin Method

1. Introduction

The Hall effect is the making of a voltage difference across an electrical conductor, transverse to an electric current in the conductor and an electromagnetic field is perpendicular to the current. It is found by Edwin Hall [1]. The problems on magnetohydrodynamics viscous fluids with hall current has importance in engineering applications

* Corresponding author.
E-mail address: jithendergurejala@gmail.com (G. Jithender Reddy).
Peer review under responsibility of Journal Transactions of A. Razmadze Mathematical Institute.

http://dx.doi.org/10.1016/j.trmi.2016.07.001

Nomenclature

List of Variables:

B_0	Uniform applied magnetic field (T)
x', y', z'	Co-ordinate system (m)
x, y, z	Dimensionless coordinates (m)
u'	Fluid velocity along the x'-axis (m s^{-1})
w'	Fluid velocity along the z'-axis (m s^{-1})
u	Non-dimensional fluid velocity along the x'-axis (m)
w	Non-dimensional fluid velocity along the z'-axis (m)
t_0	Characteristic time (s)
Nu	Nusselt number or rate of heat transfer coefficient
Sh	Sherwood number or rate of mass transfer coefficient
c_p	Specific heat at constant pressure (J kg^{-1}K)
Gr	Grashof number for heat transfer
Gm	Grashof number for mass transfer
$\bar{g}$	Acceleration due to gravity, 9.81 (m/s^2)
g	Acceleration due to gravity in magnitude (m/s^2)
K_1	Permeability parameter (K d^{-2})
k_T	Thermal diffusion ratio
T_m	Mean fluid temperature (K)
C_s	Concentration susceptibility (m mol^{-1})
k^*	Mean absorption coefficient (m^{-1})
$\bar{B}$	Magnetic induction vector
M^2	Magnetic parameter
Pr	Prandtl number
p	Fluid pressure (N m^{-2})
q_r	Radiative flux (kg/s^3)
m	Hall current parameter
N	Radiation parameter
Sr	Soret number
C'	Species concentration (kg m^{-3})
C'_∞	Species concentration of the fluid far away from the plate (kg m^{-3})
C'_w	Species concentration at the plate (kg m^{-3})
D_m	Molecular mass diffusivity (m^2 s^{-1})
D_T	Molecular diffusivity (m^2 s^{-1})
E	Electric field (S m^{-1})
Dr	Dufour number
Sc	Schmidt Number
T'_w	Temperature at the plate (K)
T'_∞	Temperature of the fluid far away from the plate (K)
t'	Time (s)
T'	Fluid temperature (K)
U_0	Plate velocity (m s^{-1})
T	Non-dimensional temperature (K)
C	Non-dimensional species concentration (kg m^{-3})

Greek symbols:

ρ	Fluid density (kg m^{-3})

κ	Thermal conductivity (W m^{-1} K^{-1})
σ	Electrical conductivity (S m^{-1})
ν	Kinematic viscosity (m^2 s^{-1})
β'	Coefficient of volume expansion for heat transfer (K^{-1})
Ω	Rotation parameter (degrees)
Ω'	Uniform angular velocity (degrees)
β^*	Coefficient of volume expansion for mass transfer (m^3 kg^{-1})
τ_x	Skin-friction in x'-direction (Pa)
τ_z	Skin-friction in z'-direction (Pa)
σ^*	Stefan–Boltzmann constant (W m^{-2} K^{-4})

Superscript

/	Dimensionless properties

Subscripts

w	Wall conditions
∞	Free stream conditions
p	Plate

such as MHD generators and MHD accelerators, laboratory plasmas, the rotating flow of fluids in the presence of magnetic field occurring in geophysical and cosmical fluid dynamics, the solar physics involved in the sunspot development, solar cycle and structure of rotating magnetic stars. The effect of Hall current with rotating system on MHD convection flows have been carried out by many researchers due to application of such studies as in the problems of MHD generators and Hall accelerators. Ajay Kumar Singh et al. [2], Mbeledogu and Ogulu [3], Abuga et al. [4], Jain and Singh [5] have studied rotation/Hall effects on various problems. Ahmed and Dutta [6] discussed transient mass transfer flow past an impulsively started infinite vertical plate in ramped plate velocity and ramped temperature. Seth et al. [7] studied the effects of hall current and rotation on natural convection radiative heat and mass transfer MHD flow past a moving vertical plate for ramped and isothermal plate only in case of externally cooling of the plate by Laplace transform technique with the absence of thermal diffusion and diffusion thermo. Chamkha et al. [8] investigated the influence of hall current on unsteady MHD free convective heat and mass transfer on a vertical porous plate with thermal radiation and chemical reaction. Sivaiah and Srinivasa Raju [9] studied the effects of Hall current and Heat source on MHD heat and mass transfer free convective flow in the presence of viscous dissipation by applying finite element technique. Siva Reddy and Srinivasa Raju [10] studied the effect of viscous dissipation on transient free convection flow past an infinite vertical plate through porous medium in the presence of magnetic field using finite element technique. Anand Rao et al. [11] demonstrated transient flow past an impulsively started infinite flat porous plate in a rotating fluid in the presence of magnetic field with Hall current using finite element technique. Anand Rao et al. [12] investigated the combined effects of heat and mass transfer on unsteady MHD flow past a vertical oscillatory plate suction velocity using finite element method. The combined effects of heat and mass transfer on unsteady MHD natural convective flow past an infinite vertical plate enclosed by porous medium in presence of thermal radiation and Hall Current was investigated by Ramana Murthy et al. [13]. Jithender Reddy et al. [14]. Anand Rao [15] and Srinivasa Raju et al. [16] studied MHD free convection fluid flow problems with various physical conditions using Finite Element Technique. Sheikholeslami et al. [17] investigated the effect of space dependent magnetic field on free convection Fe_3O_4–water nanofluid through control volume based finite element technique. Sheikholeslami et al. [18] employed control volume-based finite element technique to simulate Fe_3O_4–water nanofluid mixed convection heat transfer in a lid-driven semi annulus in the presence of a non-uniform magnetic field. Rashidi et al. [19] investigated the numerical study of magnetic field impact on mixed convection heat transfer of nanofluid in a channel with sinusoidal walls. Rashidi et al. [20] studied the combined heat and mass transfer of magnetohydrodynamic (MHD) convective and slip flow due to a rotating disk with influence of viscous dissipation and Ohmic heating by using the combination of the DTM and the Padé approximants.

The heat and mass transfer simultaneously affect each other and these will cause the cross-diffusion effect. The heat transfer caused by concentration (mass) gradient is called the diffusion-thermo (Dufour effect). On the other hand mass transfer caused by the temperature gradient is called thermal-diffusion (Soret) effect. Alam and Rahman et al. [21] investigated the Dufour (thermal-diffusion) and Soret (diffusion-thermo) effects on mixed convection flow past a vertical porous flat plate with the presence of variable suction. El-Arabawy et al. [22] investigated the Soret and Dufour effect on heat and mass transfer by natural convection from vertical surface embedded in a fluid-saturated porous media considered with variable surface temperature and constant concentration. Kafoussias et al. [23] studied thermal-diffusion and diffusion-thermo effects on mixed natural-forced convective and mass transfer boundary layer flow with the temperature dependent viscosity. Nabil et al. [24] studied thermal diffusion and diffusion thermo effects on the viscous fluid flow with heat and mass transfer through porous medium on a shrinking sheet. Srinivas et al. [25] found thermal diffusion and diffusion thermo effects on MHD viscous fluid flow between expanding rotating porous disks with viscous dissipation. Srinivasacharya et al. [26–28], Ram Reddy et al. [29] and Jithender Reddy et al. [30] studied Soret and Dufour effects on MHD free convection problems with varied physical parameters. Ahmed et al. [31] studied the effect of Soret (thermal diffusion) on unsteady free convective flow of an electrically conducting fluid over an infinite vertical oscillating plate embedded in a porous medium in the presence of a uniform transverse magnetic field. Srinivasa Raju [32] studied the combined effects of thermal-diffusion and diffusion-thermo on unsteady free convection fluid flow past an infinite vertical porous plate in the presence of magnetic field and chemical reaction using finite element technique. Srinivasa Raju et al. [33] found the numerical results for the effects of thermal radiation and heat source on an unsteady free convective flow past an infinite vertical plate with transverse magnetic field in the presence of thermal-diffusion and diffusion-thermo. Srinivasa Raju et al. [34] studied application of finite element method to unsteady MHD free convection flow past a vertically inclined porous plate including thermal diffusion and diffusion thermo effects. The influence of viscous dissipation on free convective flow past a semi-infinite vertical plate in the presence of Soret and Magnetic field was studied by Siva Reddy Sheri et al. [35]. Abdelraheem et al. [36] studied double-diffusive free convective flow over a vertical stretching surface embedded in a porous medium in the presence of a homogeneous first-order chemical reaction, radiation and Soret and Dufour effects. A numerical model was developed by Ahmed and Sibanda [37] for the effects of variable viscosity, and Soret and Dufour numbers on MHD mixed convective flow, heat and mass transfer from an exponentially stretching vertical surface embedded in a porous medium.

In this paper, we studied the hall current and rotation effects on MHD free convection flow past a moving vertical plate with the presence of thermal diffusion and diffusion thermo for isothermal and ramped temperature in both cases externally heating and cooling of the plate. The governing partial differential equations are solved by Element Free Galerkin Method and shown the present results are in good agreement with the results of Seth et al. [7].

2. Mathematical modeling

Consider an unsteady MHD natural convection flow with heat and mass transfer of an optically thick radiating, incompressible and electrically conducting viscous fluid past an infinite vertical plate is embedded in a uniform porous medium with a rotating system taking Hall current into account. Consider x'-axis is along the plate in upward direction and y'-axis is normal to plane of the plate in the fluid. A uniform transverse magnetic field B_0 is applied in a direction which is parallel to y'-axis. The fluid and plate rotate with uniform angular velocity Ω' about the y'-axis. Initially i.e. at time $t' \leq 0$, both the fluid and plate are in rest and these are maintained at a uniform temperature T'_∞. Also species concentration is at the surface of the plate as well as at every point within the fluid and it is maintained at uniform concentration C'_∞. At time $t' > 0$, plate starts moving in x'-direction with uniform velocity U_0 in its own plane. The temperature of the plate is raised or lowered to $T'_\infty + (T'_w - T'_\infty)t'/t_0$ when $0 < t' \leq t_0$, and it is maintained at uniform temperature T'_w when $t' > t_0$.

Also, at time $t' > 0$, species concentration is at the surface of the plate, it is raised to uniform species concentration C'_w and it is maintained thereafter. Geometry of the problem is shown in Fig. 1. Since plate is an infinite extent in x' and z' directions and it is electrically non-conducting, all physical quantities except pressure depends on y' and t' only. Also, no applied or polarized voltages are assumed to exist, so that the effect of polarization of fluid is negligible. The induced magnetic field generated by fluid motion is negligible in comparison to the applied one. This assumption is justified because magnetic Reynolds number is very small for liquid metals and partially ionized fluids which are commonly used in industrial applications (Cramer and Pai [38]). Keeping in view of these assumptions and under the

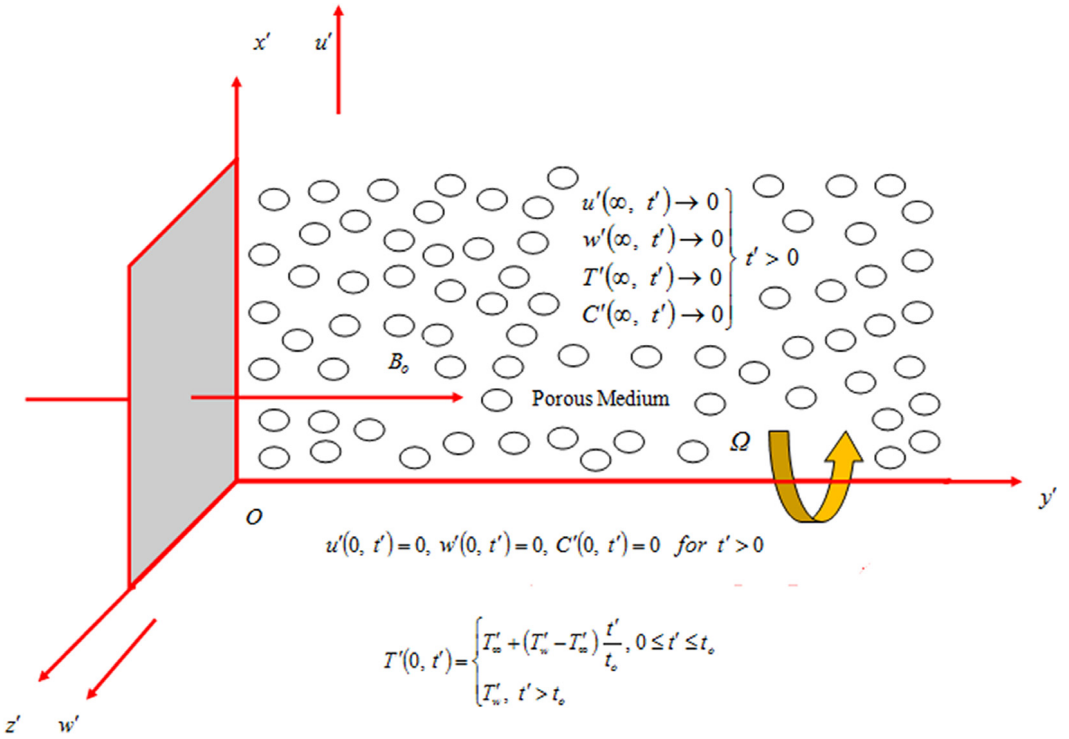

Fig. 1. Geometry of the problem.

Boussinesq's approximation, the governing equations are given by (Seth et al. [7])

$$\frac{\partial u'}{\partial t'} + 2\Omega' w' = \nu \frac{\partial^2 u'}{\partial y'^2} - \frac{\sigma B_o^2}{\rho\left(1+m^2\right)}\left(u' + m w'\right) - \frac{\nu u'}{K_1} + g\beta'\left(T' - T'_\infty\right) + g\beta^*\left(C' - C'_\infty\right) \tag{1}$$

$$\frac{\partial w'}{\partial t'} - 2\Omega' u' = \nu \frac{\partial^2 w'}{\partial y'^2} - \frac{\sigma B_o^2}{\rho\left(1+m^2\right)}\left(m u' - w'\right) - \frac{\nu w'}{K_1} \tag{2}$$

$$\frac{\partial T'}{\partial t'} = \frac{\kappa}{\rho c_p}\frac{\partial^2 T'}{\partial y'^2} - \frac{1}{\rho c_p}\frac{\partial q_r}{\partial y'} + \frac{D_m k_T}{c_s c_p}\frac{\partial^2 C'}{\partial y'^2} \tag{3}$$

$$\frac{\partial C'}{\partial t'} = D\frac{\partial^2 C'}{\partial y'^2} + \frac{D_m k_T}{T_m}\frac{\partial^2 T'}{\partial y'^2}. \tag{4}$$

The boundary conditions for the primary and secondary velocity, temperature and concentration fields are (Seth et al. [7])

$$\forall t' \le 0 : u' = w' = 0,\ T' = T'_\infty,\ C' = C'_\infty \text{ for } y' \ge 0 \tag{5}$$

$$\forall t' > 0 : u' = U_0,\ w' = 0,\ C' = C'_w \text{ at } y' = 0 \tag{6}$$

$$T' = T'_\infty + (T'_w - T'_\infty)t'/t_0 \text{ at } y' = 0 \text{ for } 0 < t' \le t_0 \tag{7}$$

$$\forall t' > t_0 : T' = T'_w \text{ at } y' = 0 \tag{8}$$

$$\forall t' > 0 : u' = 0, w' = 0,\ T' \to T'_\infty,\ C' \to C'_\infty \text{ at } y' \to \infty. \tag{9}$$

The radiative heat flux term by using the Rosseland approximation (Sparrow and Cess [39]) is given by

$$q'_r = -\frac{4\sigma^*}{3k^*}\left(\frac{\partial T'^4}{\partial y'}\right)_{y=0}. \tag{10}$$

It should be noted that by using the Rosseland approximation, present analysis is limited to optically thick fluids. If temperature differences within the flow are sufficiently very small then Eq. (10) can be linearized by expanding T' into the Taylor series about T'_∞ which after neglecting higher order terms take the form

$$T'^4 \cong 4T'^3_\infty - 3T'^4_\infty. \tag{11}$$

Substituting Eqs. (10) and (11), into Eq. (3), we obtain

$$\frac{\partial T'}{\partial t'} = \frac{\kappa}{\rho c_p}\frac{\partial^2 T'}{\partial y'^2} + \frac{1}{\rho c_p}\frac{16\sigma^* T'^3_\infty}{3k^*}\frac{\partial^2 T'}{\partial y'^2} + \frac{D_m k_T}{c_s c_p}\frac{\partial^2 C'}{\partial y'^2}. \tag{12}$$

Introducing the following non-dimensional quantities into the Eqs. (1), (2), (4), (12) and (5)–(9)

$$u = \frac{u'}{U_0},\ w = \frac{w'}{U_0},\ y = \frac{y' U_0}{\nu},\ t = \frac{t' U_0^2}{\nu},\ T = \frac{T' - T'_\infty}{T'_w - T'_\infty},\ C = \frac{C' - C'_\infty}{C'_w - C'_\infty},$$
$$M^2 = \frac{\sigma B_0^2 \nu}{\rho U_0^2},\ \Omega = \frac{\nu \Omega'}{U_0^2},\ K_1 = \frac{K'_1 U_0^2}{\nu^2},\ Gr = \frac{g\beta\nu(T'_w - T'_\infty)}{U_0^3},$$
$$Gm = g\beta^*\nu\frac{C'_w - C'_\infty}{U_0^3},\ Pr = \frac{\nu\rho c_p}{\kappa},\ N = \frac{16\sigma^* T'^3_\infty}{3\kappa k^*},\ S_c = \frac{\nu}{D},$$
$$Sr = \frac{D_m k_T (T'_w - T'_\infty)}{\nu T_m (C'_w - C'_\infty)},\ Dr = \frac{D_m k_T (C'_w - C'_\infty)}{\nu c_s c_p (T'_w - T'_\infty)}$$

then the resultant non-dimensional equations are

$$\frac{\partial u}{\partial t} + 2\Omega w = \frac{\partial^2 u}{\partial y^2} - M^*(u + mw) - \frac{u}{K_1} + GrT + GmC \tag{13}$$

$$\frac{\partial w}{\partial t} - 2\Omega u = \frac{\partial^2 w}{\partial y^2} + M^*(mu - w) - \frac{w}{K_1} \tag{14}$$

$$\frac{\partial T}{\partial t} = R\frac{\partial^2 T}{\partial y^2} + Dr\frac{\partial^2 C}{\partial y^2} \tag{15}$$

$$\frac{\partial C}{\partial t} = \frac{1}{Sc}\frac{\partial^2 C}{\partial y^2} + Sr\frac{\partial^2 T}{\partial y^2} \tag{16}$$

where $M^* = \frac{M^2}{1+m^2}$, $R = \frac{1+N}{Pr}$.

The non-dimensional initial and boundary conditions are

$$\forall t \le 0 : u = w = 0,\ T = 0, C = 0 \text{ for } y \ge 0 \tag{17}$$
$$\forall t > 0 : u = 1,\ w = 0,\ C = 1 \text{ at } y = 0 \tag{18}$$
$$\forall 0 < t \le 1 : T = t \text{ at } y = 0 \tag{19}$$
$$\forall t > 1 : T = 1 \text{ at } y = 0 \tag{20}$$
$$\forall t > 0 :\ u \to 0,\ w \to 0,\ T \to 0,\ C \to 0 \text{ at } y \to \infty. \tag{21}$$

3. Numerical solution by Element Free Galerkin Method (EFGM)

Element Free Galerkin Method (EFGM) is one of the computational method developed by Belytschko et al. [40]. This method is applicable to arbitrary shapes, and it requires only nodal data which is applied to elasticity and heat conduction problems. This method shares essential characteristics with many other numerical methods such as Kernal particle method (Liu et al. [41]), Finite point method (Onate et al. [42]) and Hp-clouds (Duarte and Oden et al. [43]). Previously, the review of these numerical methods was reported by Belytschko et al. [44]. Recently, several authors applied this EFGM in their research problems. In spite of that, Rajesh Sharma and Bhargava [45] found the numerical

solutions of unsteady MHD convection heat and mass transfer past a semi-infinite vertical porous moving plate using EFGM. Ryszard [46] applied an EFGM to water wave propagation problems. Very recently, Singh and Bhargava [47] studied the characteristics of heat transfer flow of a phase transition in melting problem using FEM and EFGM, and the results are shown closer to each other. Rajesh Sharma [48] found the numerical simulation of MHD Hiemenz flow of a micropolar fluid on non linear stretching sheet embedded in porous Medium using EFGM. Srinivasa Raju et al. [49] found the numerical and analytical solutions of unsteady MHD free convection on exponential accelerated vertical plate with heat absorption using Element Free Galerkin Method and Laplace Transform Technique respectively. Also they have shown the numerical solutions by FEM are in good agreement with the analytical solutions by LTT.

3.1. Review of Element Free Galerkin Method

The Element Free Galerkin Method (EFGM) requires moving least square (MLS) interpolation functions to approximate an unknown function, which is made up of three components: a weight function associated with each node, a basis function and a set of coefficients that depends on position. The weight function is non-zero over a small neighborhood at a particular node, called support of the node. Using MLS approximation, the unknown velocity component u is approximated over the domain $[0, \infty]$ as

$$u(x) \cong u^h(x) = \sum_{j=1}^{m} p_j(x)\, a_j(x) = p^T(x)\; a(x) \tag{22}$$

where m is the number of terms in the basis, $p_j(x)$ the monomial basis function, $a_j(x)$ the non-constant coefficients and $p^T(x) = [1x]$. The coefficients $a_j(x)$ are determined by minimizing the functional $J(x)$ given by

$$J(x) = \sum_{i=1}^{m} w(x - x_i) \left\{ \sum_{j=1}^{m} p_j(x_i)\, a_j(x) - u_i \right\}^2 \tag{23}$$

where $w(x - x_i)$ is a weight function which is non-zero over a small domain, called domain of influence, n is the number of nodes in the domain of influence. The minimization of $J(x)$ w.r.t $a(x)$ leads to the following set of equation

$$a(x) = C^{-1}(x)\, D(x)\, U^T \tag{24}$$

where C and D are given as

$$C = \sum_{i=1}^{n} w(x - x_i)\, p(x_i)\, p^T(x_i) \tag{25}$$

$$D(x) = [w(x - x_1)\, p(x_1), w(x - x_2)\, p(x_2), w(x - x_3)\, p(x_3), \ldots, w(x - x_n)\, p(x_n)] \tag{26}$$

$$U^T = [U_1, U_2, U_3, \ldots, U_n]. \tag{27}$$

Substituting Eq. (24) in Eq. (22), the MLS approximants are obtained as

$$u(x) \cong u^h(x) = \sum_{i=1}^{n} \Phi_i(x)\, u_i = \Phi(x)\, u. \tag{28}$$

Similarly $\theta(x), \phi(x)$ can be approximated by

$$\theta(x) \cong \theta^h(x) = \sum_{i=1}^{n} \Phi_i(x)\, \theta_i = \Phi(x)\, \theta \tag{29}$$

$$\phi(x) \cong \phi^h(x) = \sum_{i=1}^{n} \Phi_i(x)\, \phi_i = \Phi(x)\, \phi \tag{30}$$

where the shape function $\Phi_i(x)$ is defined by

$$\Phi_i(x) = \sum_{j=1}^{n} p_j(x) \left(C^{-1}(x) D(x)\right)_{ji} = p^T C^{-1} D_i. \tag{31}$$

3.2. Choice of weight function

The weight function is non-zero over a small neighborhood of x_i, called the domain of the influence of node i. The choice of weight function $w(x - x_i)$ affects the resulting approximation in EFGM and other mesh less methods. Singh et al. [50] studied these weight functions and found that cubicspline weight function gives more accurate results as compared to others. Therefore, in the present work, a cubicspline weight function (Singh et al. [50]) has been used.

3.3. Cubic spline weight function

$$w(r - r_i) = w(r) = \begin{cases} \frac{2}{3} - 4r^2 + 4r^3 & \text{for } r \le \frac{1}{2} \\ \frac{4}{3} - 4r + 4r^2 - \frac{4}{3}r^3 & \text{for } \frac{1}{2} \le r \le 1 \\ 0 & \text{for } r > 1 \end{cases} \tag{32}$$

where $r_i = \frac{\|x - x_i\|}{d_{ml}}$, d_{ml} are the size of domain of influence which are calculated as $d_{ml} = d_{\max} C_i$, where $d_{\max}$ is a scaling parameter, and C_i is the distance to the nearest neighbors. The size of the domain of influence (d_{ml}) at particular node i is only controlled by scaling parameter ($d_{\max}$) since the distance between nearest neighbors for an evaluation point remains unchanged for a given nodal data distribution. The minimum value of $d_{\max}$ should be greater than 1 so that $n > m$, and the maximum value of $d_{\max}$ should be such that it preserves the local character of MLS approximation. It has been shown in Singh [51] that $1 < d_{\max} < 1.5$ is the optimum range of scaling parameter for heat transfer problem. Therefore $d_{\max}$ has been fixed as 1.01.

The weighted integral forms of Eqs. (13)–(16) can be written as

$$\int_0^{y_{\max}} w_1 \left[\frac{\partial^2 u}{\partial y^2} - \left(\frac{\partial u}{\partial t}\right) - Nu - M^* m w - 2\Omega w + GrT + GmC\right] dy = 0 \tag{33}$$

$$\int_0^{y_{\max}} w_2 \left[\frac{\partial^2 w}{\partial y^2} - \left(\frac{\partial w}{\partial t}\right) - Nw + \left(M^*\right)(m)(u) + 2\Omega u\right] dy = 0 \tag{34}$$

$$\int_0^{y_{\max}} w_3 \left[R\frac{\partial^2 T}{\partial y^2} - \left(\frac{\partial T}{\partial t}\right) + (Dr)\left(\frac{\partial^2 C}{\partial y^2}\right)\right] dy = 0 \tag{35}$$

$$\int_0^{y_{\max}} w_4 \left[\left(\frac{1}{Sc}\right)\frac{\partial^2 C}{\partial y^2} - \left(\frac{\partial C}{\partial t}\right) + (Sr)\left(\frac{\partial^2 T}{\partial y^2}\right)\right] dy = 0 \tag{36}$$

where $N = M^* + \frac{1}{K_1}$ and w_1, w_2, w_3, w_4 are arbitrary test functions and may be viewed as the variations in u, w, T and C, respectively. After reducing the order of integration and non-linearity, the following system of equations are obtained:

$$\int_0^{y_{\max}} \left[\left(\frac{\partial w_1}{\partial y}\right)\left(\frac{\partial u}{\partial y}\right) + (w_1)\left(\frac{\partial u}{\partial t}\right) + N(w_1)u + M^* m(w_1)w + 2\Omega(w_1)w + (Gr)(w_1)T - (Gm)(w_1)C\right] dy - \left[(w_1)\left(\frac{\partial u}{\partial y}\right)\right]_0^{y_{\max}} = 0 \tag{37}$$

$$\int_0^{y_{\max}} \left[\left(\frac{\partial w_2}{\partial y}\right)\left(\frac{\partial w}{\partial y}\right) + (w_2)\left(\frac{\partial w}{\partial t}\right) + N(w_2)w - M^* m(w_2)u - 2\Omega(w_2)w\right] dy - \left[(w_2)\left(\frac{\partial w}{\partial y}\right)\right]_0^{y_{\max}} = 0 \tag{38}$$

$$\int_0^{y_{\max}} \left[R\left(\frac{\partial w_3}{\partial y}\right)\left(\frac{\partial T}{\partial y}\right) + (w_3)\left(\frac{\partial T}{\partial t}\right) + (Dr)(w_3)\left(\frac{\partial w_3}{\partial y}\right)\left(\frac{\partial C}{\partial y}\right)\right] dy$$
$$- \left[R(w_3)\left(\frac{\partial T}{\partial y}\right) + (Dr)(w_3)\left(\frac{\partial C}{\partial y}\right)\right]_0^{y_{\max}} = 0 \tag{39}$$

$$\int_0^{y_{\max}} \left(\frac{1}{Sc}\right)\left[\left(\frac{\partial w_4}{\partial y}\right)\left(\frac{\partial C}{\partial y}\right) + (w_4)\left(\frac{\partial C}{\partial t}\right) + (Sr)(w_4)\left(\frac{\partial w_4}{\partial y}\right)\left(\frac{\partial T}{\partial y}\right)\right] dy$$
$$- \left[(w_4)\left(\frac{1}{SC}\right)\left(\frac{\partial C}{\partial y}\right) + (Sr)(w_4)\left(\frac{\partial T}{\partial y}\right)\right]_0^{y_{\max}} = 0. \tag{40}$$

Using the essential boundary conditions on w_1, w_2, w_3, w_4 as homogeneous, Eqs. (37)–(40) become

$$\int_0^{y_{\max}} \left[\left(\frac{\partial w_1}{\partial y}\right)\left(\frac{\partial u}{\partial y}\right) + (w_1)\left(\frac{\partial u}{\partial t}\right) + N\left(w_1\right)u + M^*m(w_1)w$$
$$+ 2\Omega(w_1)w - (Gr)(w_1)T - (Gm)(w_1)C\right] dy = 0 \tag{41}$$

$$\int_0^{y_{\max}} \left[\left(\frac{\partial w_2}{\partial y}\right)\left(\frac{\partial w}{\partial y}\right) + (w_2)\left(\frac{\partial w}{\partial t}\right) + N(w_2)w - M^*m(w_2)u - 2\Omega(w_2)w\right] dy = 0 \tag{42}$$

$$\int_0^{y_{\max}} \left[R\left(\frac{\partial w_3}{\partial y}\right)\left(\frac{\partial T}{\partial y}\right) + (w_3)\left(\frac{\partial T}{\partial t}\right) + (Dr)(w_3)\left(\frac{\partial w_3}{\partial y}\right)\left(\frac{\partial C}{\partial y}\right)\right] dy = 0 \tag{43}$$

$$\int_0^{y_{\max}} \left(\frac{1}{Sc}\right)\left[\left(\frac{\partial w_4}{\partial y}\right)\left(\frac{\partial C}{\partial y}\right) + (w_4)\left(\frac{\partial C}{\partial t}\right) + (Sr)(w_4)\left(\frac{\partial w_4}{\partial y}\right)\left(\frac{\partial T}{\partial y}\right)\right] dy = 0. \tag{44}$$

3.4. Essential boundary conditions

Due to lack of Kronecker delta property in EFGM, the shape function Φ_i possesses some difficulty in the imposition of essential boundary conditions. To remove this problem, different numerical techniques have been proposed to enforce the essential boundary condition in EFGM such as Lagrange multiplier technique, modified variational principle approach and penalty approach. The penalty method Zhu and Atluri [52] is applied which is discussed as follows:

Penalty Method (PM):

$$\int_0^{y_{\max}} \left[\left(\frac{\partial w_1}{\partial y}\right)\left(\frac{\partial u}{\partial y}\right) + (w_1)\left(\frac{\partial u}{\partial t}\right) + N(w_1)u + M^*m(w_1)w + 2\Omega(w_1)w - (Gr)(w_1)T\right.$$
$$\left. - (Gm)(w_1)C\right] dy - \alpha(w_1)(u-u_o)|_{y=0} - \alpha(w_1)(u-u_\infty)|_{y\to\infty} = 0 \tag{45}$$

$$\int_0^{y_{\max}} \left[\left(\frac{\partial w_2}{\partial y}\right)\left(\frac{\partial w}{\partial y}\right) + (w_2)\left(\frac{\partial w}{\partial t}\right) + N(w_2)w - M^*m(w_2)u - 2\Omega(w_2)u\right] dy$$
$$- \alpha(w_2)(w-w_o)|_{y=0} - \alpha(w_2)(w-w_\infty)|_{y\to\infty} = 0 \tag{46}$$

$$\int_0^{y_{\max}} \left[R\left(\frac{\partial w_3}{\partial y}\right)\left(\frac{\partial T}{\partial y}\right) + (w_3)\left(\frac{\partial T}{\partial t}\right) + (Dr)(w_3)\left(\frac{\partial w_3}{\partial y}\right)\left(\frac{\partial C}{\partial y}\right)\right] dy$$
$$- \alpha(w_3)(T-T_o)|_{y=0} - \alpha(w_3)(T-T_\infty)|_{y\to\infty}$$
$$- \alpha(Dr)(w_3)(C-C_o)|_{y=0} - \alpha(Dr)(w_3)(C-C_\infty)|_{y\to\infty} = 0 \tag{47}$$

$$\int_0^{y_{\max}} \left(\frac{1}{SC}\right)\left[\left(\frac{\partial w_4}{\partial y}\right)\left(\frac{\partial C}{\partial y}\right)+(w_4)\left(\frac{\partial C}{\partial t}\right)+(Sr)\,(w_4)\left(\frac{\partial w_4}{\partial y}\right)\left(\frac{\partial T}{\partial y}\right)\right]dy$$

$$-\alpha\frac{\alpha}{Sc}\,(w_4)\,(C-C_o)\Big|_{y=0}-\alpha\frac{\alpha}{Sc}\,(w_4)\,(C-C_\infty)\Big|_{y\to\infty}$$

$$-\alpha\,(Sr)\,(w_4)\,(T-T_o)|_{y=0}-\alpha\,(Sr)\,(w_4)\,(T-T_\infty)|_{y\to\infty}=0 \tag{48}$$

where $\left.\begin{array}{l} u_o=1,\ w_o=0, T_o=t \text{ at } 0<t\le 1,\\ T_o=1 \text{ at } t>1\\ C_o=1,\ u_\infty=1,\ w_\infty=0,\ T_\infty=0,\ C_\infty=0\end{array}\right\}$ and $w_1=w_2=w_3=w_4=\Phi_i\ (i=1,2,\ldots,n)$.

Thus, Eqs. (45)–(48) can be written as:

$$[K]\left\{\bar{h}\right\}+\left[\bar{M}\right]\left\{\dot{\bar{h}}\right\}=\{F\} \tag{49}$$

where $[K]=\begin{bmatrix}K_{11}&K_{12}&K_{13}&K_{14}\\K_{21}&K_{22}&K_{23}&K_{24}\\K_{31}&K_{32}&K_{33}&K_{34}\\K_{41}&K_{42}&K_{43}&K_{44}\end{bmatrix}$, $\left[\bar{M}\right]=\begin{bmatrix}Mooo\\oMoo\\ooMo\\oooM\end{bmatrix}$, $\left\{\bar{h}\right\}=\begin{bmatrix}\{u\}\\\{w\}\\\{T\}\\\{C\}\end{bmatrix}$, $\left\{\dot{\bar{h}}\right\}=\begin{bmatrix}\{\dot{u}\}\\\{\dot{w}\}\\\{\dot{T}\}\\\{\dot{C}\}\end{bmatrix}$, $\{F\}=\begin{bmatrix}\{F_1\}\\\{F_2\}\\\{F_3\}\\\{F_4\}\end{bmatrix}$,

$$(K_{11})_{ij}=\int_0^{y_{\max}}\left[\left(\Phi_i^{T\prime}\right)\left(\Phi_j'\right)\right]dy+N\int_0^{y_{\max}}\left[\left(\Phi_i^T\right)\left(\Phi_j\right)\right]dy$$
$$-\left[\alpha\left(\Phi_i^T\right)\left(\Phi_j\right)\right]_{y=0}-\left[\alpha\left(\Phi_i^T\right)\left(\Phi_j\right)\right]_{y\to\infty},$$

$$(K_{12})_{ij}=\left(M^*m+2\Omega\right)\int_0^{y_{\max}}\left[\left(\Phi_i^T\right)\left(\Phi_j\right)\right]dy,\ (K_{13})_{ij}=-(Gr)\int_0^{y_{\max}}\left(\Phi_i^T\right)\left(\Phi_j\right)dy,$$

$$(K_{14})_{ij}=-(Gm)\int_0^{y_{\max}}\left(\Phi_i^T\right)\left(\Phi_j\right)dy,\ (M)_{ij}=\int_0^{y_{\max}}\left(\Phi_i^T\right)\left(\Phi_j\right)dy,\ \forall i=j, (M)_{ij}=0, \forall i\neq j$$

$$(K_{21})_{ij}=\left(M^*m+2\Omega\right)\int_0^{y_{\max}}\left[\left(\Phi_i^T\right)\left(\Phi_j\right)\right]dy,$$

$$(K_{22})_{ij}=\int_0^{y_{\max}}\left[\left(\Phi_i^{T\prime}\right)\left(\Phi_j'\right)\right]dy+N\int_0^{y_{\max}}\left[\left(\Phi_i^T\right)\left(\Phi_j\right)\right]dy-\left[\alpha\left(\Phi_i^T\right)\left(\Phi_j\right)\right]_{y=0}$$
$$-\left[\alpha\left(\Phi_i^T\right)\left(\phi_j\right)\right]_{y\to\infty},$$

$$(K_{23})_{ij}=(K_{24})_{ij},\ (K_{31})_{ij}=0=(K_{32})_{ij},$$

$$(K_{33})_{ij}=-R\int_0^{y_{\max}}\left[\left(\Phi_i^{T\prime}\right)\left(\Phi_j'\right)\right]dy+\left[R\alpha\left(\Phi_i^T\right)\left(\Phi_j\right)\right]_{y=0}-\left[R\alpha\left(\Phi_i^T\right)\left(\Phi_j\right)\right]_{y\to\infty},$$

$$(K_{34})_{ij}=(Dr)\int_0^{y_{\max}}\left[\left(\Phi_i^{T\prime}\right)\left(\Phi_j'\right)\right]dy-\left[\alpha\,(Dr)\left(\Phi_i^T\right)\left(\Phi_j\right)\right]_{y=0}-\left[\alpha\,(Dr)\left(\Phi_i^T\right)\left(\Phi_j\right)\right]_{y\to\infty},$$

$$(K_{41})_{ij}=0=(K_{42})_{ij},$$

$$(K_{43})_{ij}=(Sr)\int_0^{y_{\max}}\left[\left(\Phi_i^{T\prime}\right)\left(\Phi_j'\right)\right]dy-\left[\alpha\,(Sr)\left(\Phi_i^T\right)\left(\Phi_j\right)\right]_{y=0}-\left[\alpha\,(Sr)\left(\Phi_i^T\right)\left(\Phi_j\right)\right]_{y\to\infty},$$

$$(K_{44})_{ij}=\frac{1}{Sc}\int_0^{y_{\max}}\left[\left(\Phi_i^{T\prime}\right)\left(\Phi_j'\right)\right]dy-\left[\frac{\alpha}{Sc}\left(\Phi_i^T\right)\left(\Phi_j\right)\right]_{y=0}-\left[\frac{\alpha}{Sc}\left(\Phi_i^T\right)\left(\Phi_j\right)\right]_{y\to\infty},$$

$$(F_1)_i=u_o\alpha\,\Phi_j'+u_\infty\alpha\,\Phi_j',\ (F_2)_i=w_o\alpha\,\Phi_j'+w_\infty\alpha\,\Phi_j',$$

$$(F_3)_i=T_o\alpha\,\Phi_j'+T_\infty\alpha\,\Phi_j' \text{ at } 0<t\le 1,\ (F_3)_i=T_o\alpha\,\Phi_j'+T_\infty\alpha\,\Phi_j' \text{ at } t>1,$$

$$(F_4)_i=C_o\alpha\,\Phi_j'+C_\infty\alpha\,\Phi_j',$$

Using unconditionally stable Crank–Nicholson scheme (Smith [53]), Eq. (49) at $(s+1)$th level can be written as

$$\left[\hat{K}\right]_{s+1}\left\{\bar{h}\right\}_{s+1}=\left[\hat{K}\right]_s\left\{\bar{h}\right\}_s+\left\{\hat{F}\right\}_{s,s+1} \tag{50}$$

Table 1
The numerical values of u, w, T and C for variation of mesh sizes.

	Mesh size $h = 0.1$				Mesh size $h = 0.2$				Mesh size $h = 0.3$			
	u	w	T	C	u	w	T	C	u	w	T	C
	1.000000	0.000000	0.500000	1.000000	1.000000	0.000000	0.500000	1.000000	1.000000	0.000000	0.500000	1.000000
	0.205745	0.364936	0.329594	0.472351	0.205628	0.364842	0.329485	0.472215	0.205631	0.364853	0.329494	0.472224
	0.081102	0.102188	0.184112	0.158479	0.081852	0.102752	0.184256	0.158542	0.081851	0.102765	0.184264	0.158551
	0.026275	0.024006	0.084624	0.037798	0.026138	0.024158	0.084745	0.037813	0.026145	0.024161	0.084759	0.037824
Time	0.007119	0.004851	0.032037	0.006504	0.007015	0.004784	0.032183	0.006519	0.007019	0.004794	0.032194	0.006521
$t = 0.1$	0.001639	0.000846	0.010157	0.000824	0.001631	0.000850	0.010161	0.000891	0.001642	0.000859	0.010174	0.000912
	0.000324	0.000128	0.002747	7.86E−05	0.000324	0.000126	0.002747	7.86E−05	0.000324	0.000125	0.002758	7.86E−05
	5.54E−05	1.69E−05	0.000644	5.76E−06	5.54E−05	1.69E−05	0.000644	5.76E−06	5.54E−05	1.69E−05	0.000654	5.76E−06
	8.29E−06	1.97E−06	0.000132	3.3E−07	8.29E−06	1.97E−06	0.000132	3.3E−07	8.29E−06	1.97E−06	0.000132	3.3E−07
	1.09E−06	2E−07	2.38E−05	2E−08	1.09E−06	2E−07	2.38E−05	2E−08	1.09E−06	2E−07	2.38E−05	2E−08

where

$$\left[\hat{K}\right]_{s+1} = \left[\overline{M}\right] + \frac{\Delta t\,[K]_{s+1}}{2},\quad \left[\hat{K}\right]_{s} = \left[\overline{M}\right] - \frac{\Delta t\,[K]_{s}}{2} \text{ and } \left[\hat{F}\right]_{s,s+1} = \frac{\Delta t}{2}\left(\{F\}_{s+1} + \{F\}_{s}\right). \tag{51}$$

For computational purposes, the coordinate y is varied from 0 to $y_{\max} = 10$, where $y_{\max}$ represents infinity i.e. external to the momentum, energy and concentration boundary layers. The whole domain is divided into 101 nodes. One point Gauss quadrature formula has been used to calculate the integral values. As the systems of equations are non-linear, an iterative scheme is employed to solve the matrix system. This system is linearized by incorporating known function u, which is solved using Gauss elimination method maintaining an accuracy of 0.0000005. The code of the algorithm has been executed in MATLAB running on a PC. Excellent convergence was achieved for all the results.

3.5. Study of grid independence

In general, to study the grid independency/dependency, the mesh size should be varied in order to check the solution at different mesh (grid) sizes and get a range at which there is no variation in the solution. We have shown the numerical values of Primary velocity (u), Secondary velocity (w), temperature (T) and concentration (C) for different values of mesh (grid) size at time $t = 1.0$ in Table 1. From this table, we observed that there is no variation in the values of Primary velocity (u), Secondary velocity (w), temperature (T) and concentration (C) for different values of mesh (grid) size at time $t = 0.1$. Hence, we conclude that the results are independent of mesh (grid) size.

4. Skin-friction, rate of heat and mass transfer coefficients

The skin-friction due to primary velocity at the wall along x'-axis in dimensionless form is given by $\tau_x = \left[\frac{\partial u}{\partial y}\right]_{y=0}$.

The skin-friction due to secondary velocity at the wall along z'-axis in dimensionless form is given by $\tau_z = \left[\frac{\partial u}{\partial z}\right]_{z=0}$.

Rate of heat transfer (Nusselt number) due to temperature profiles in dimensionless form is given by $Nu = -\left[\frac{\partial T}{\partial y}\right]_{y=0}$.

And rate of mass transfer (Sherwood number) due to concentration profiles in dimensionless form is given by $Sh = -\left[\frac{\partial C}{\partial y}\right]_{y=0}$.

5. Code validation

5.1. Comparison with analytical solutions

Comparison of τ_x and τ_z with Seth et al. [7] is shown by the superscript star in Table 2. Ω is replaced by K^2 in Seth et al. [7] with varied values of Hall current and rotation parameters and in the absence of Soret and Dufour number. The present results are in good agreement with the results of Seth et al. [7] for both ramped temperature and isothermal

Table 2
The skin-friction due to primary and secondary velocity with the effect of Hall current and rotation in case of cooling of the plate.

m	Ω	τ_x (Present results)		τ_x^* (Seth et al. [7])		τ_z (Present results)		τ_z^* (Seth et al. [7])	
		Ramped	Isothermal	Ramped	Isothermal	Ramped	Isothermal	Ramped	Isothermal
0.5	5	2.87095	2.29039	2.87124	2.29044	2.35013	2.60663	2.35018	2.60816
1	5	2.49089	1.92395	2.49195	1.92406	2.85873	3.19315	2.85995	3.19048
1.5	5	2.13521	1.56012	2.13659	1.56425	3.40649	3.40037	3.06904	3.45031
0.5	3	2.61221	1.97075	2.61086	1.97001	1.86393	2.09214	1.86439	2.09575
0.5	7	3.14353	2.61096	3.14162	2.61276	2.77062	3.05629	2.77199	3.04199

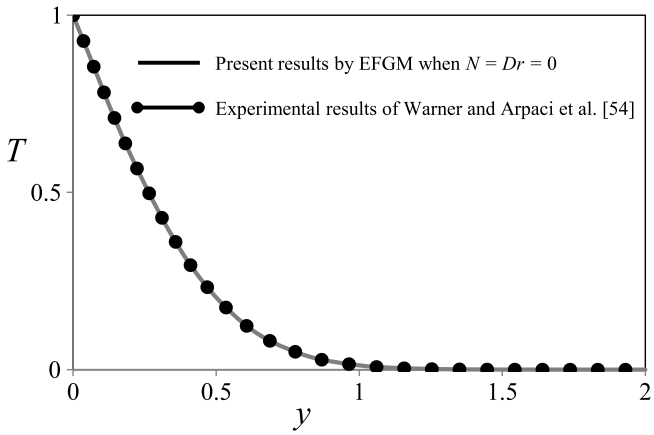

Fig. 2. Comparison of present results with existed experimental results of temperature distribution with an influence of $Pr = 0.71$.

plate in case of externally cooling of the plate. Although it is possible to obtain the exact solution using the Laplace Transform Technique (LTT), it seems to be a laborious process. The present method, EFGM is more economical and flexible in the computational point of view. Therefore, this method is superior than the LTT and other appropriate methods.

5.2. Comparison with experimental results

An experimental investigation of turbulent and laminar natural convection in air on a vertical plate is described by Warner and Arpaci [54]. But this study did not explore the experimental results with the presence of Hall current, rotation, radiation, thermal diffusion and diffusion thermo parameters. We compared the present results with the results of Warner and Arpaci [54] in the absence of these parameters. Fig. 2 shows the comparison of present results with existing experimental results of temperature distribution with an influence of $Pr = 0.71$ (Air). It is evident that the present numerical solutions are in good agreement with experimental results of Warner and Arpaci [54] in the absence of radiation and diffusion thermo parameters. These types of models are useful for validation purpose in view of lab experimental results.

6. Results and discussions

The effects of hall current and rotation on an unsteady radiative MHD free convective heat and mass transfer of an optically thick radiating, incompressible, electrically conducting and viscous fluid past an impulsively moving vertical porous plate with ramped temperature and isothermal were studied taking into account the thermal diffusion and diffusion thermo, and solved by Element Free Galerkin Method. Computations are performed for a wide range of some important governing flow physical parameters *viz.*, Hall current (m), Rotation (Ω), Soret (Sr) and Dufour (Dr).

The effects of these flow physical parameters on the primary and secondary velocity, temperature and concentration fields for ramped temperature and isothermal plates in case of both externally cooling ($Gr > 0$) and heating ($Gr < 0$) of the plate are illustrated graphically. We have shown some results are in good agreement with the results of Seth

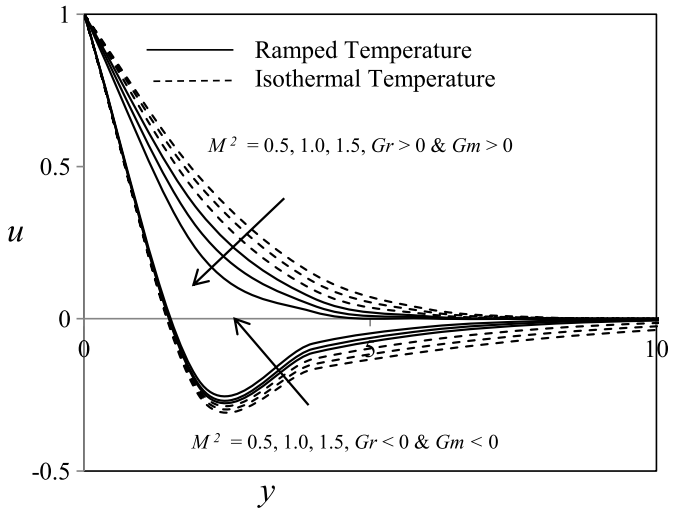

Fig. 3. Magnetic field effect M^2 on primary velocity profiles.

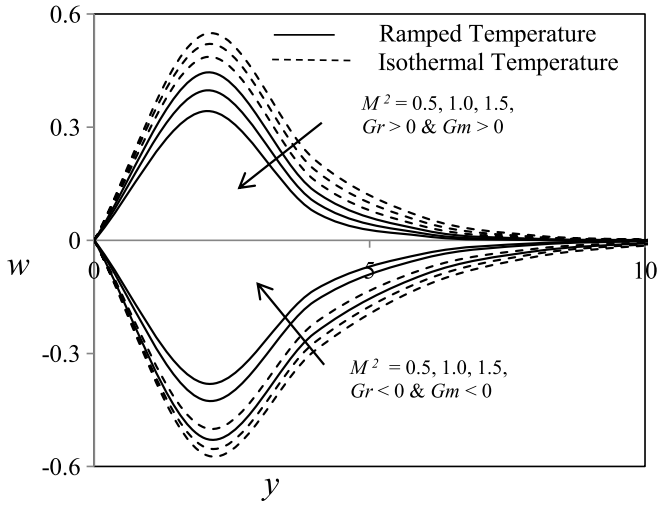

Fig. 4. Magnetic field effect M^2 on secondary velocity profiles.

et al. [7]. Some physical parameters are fixed at real constants with $Gr = 6$, $Gm = 5$, $Gr = -6$, $Gm = -5$, $M^2 = 0.5$, $m = 0.5$, $\Omega = 5$, $N = 5$, $Pr = 0.71$, $Dr = 1$, $Sc = 0.6$ and $Sr = 1$, unless specifically indicated on the appropriate graphs and tables. Figs. 3–12 display the effects of material parameters such as m, Ω, Sr and Dr on the primary and secondary velocity field for both externally cooling ($Gr > 0$) and heating ($Gr < 0$) of the plate. Figs. 13–15 display the effects of material parameters such as N, Pr, and Dr on the temperature profiles and Figs. 16 and 17 display the effects of material parameters such as Sr and Sc on the concentration field.

6.1. Primary and secondary velocity profiles

Figs. 3 and 4 show the effect of Magnetic parameter on the primary and secondary velocity for both ramped temperature and isothermal plate. The primary and secondary velocity decreases with the increase in the magnetic parameter in entire positive quadrant for both ramped and isothermal temperature with externally cooling of the plate while the effect is opposite in case of externally heating of the plate. Velocity profile decreases with increasing Magnetic parameter due to the fact that applied transverse magnetic field produces a drag in the form of Lorentz force thereby decreasing the magnitude of velocity. Figs. 5 and 6 show the effect of Hall current on the primary and secondary velocity for both ramped temperature and isothermal plate. The primary velocity and secondary velocity

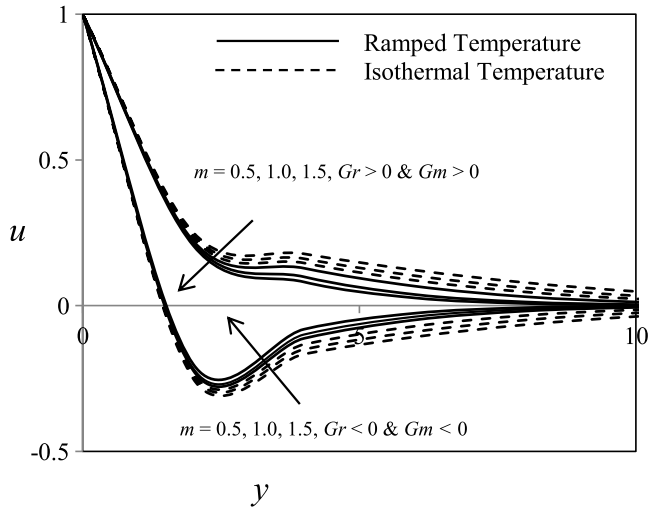

Fig. 5. Hall effect m on primary velocity profiles.

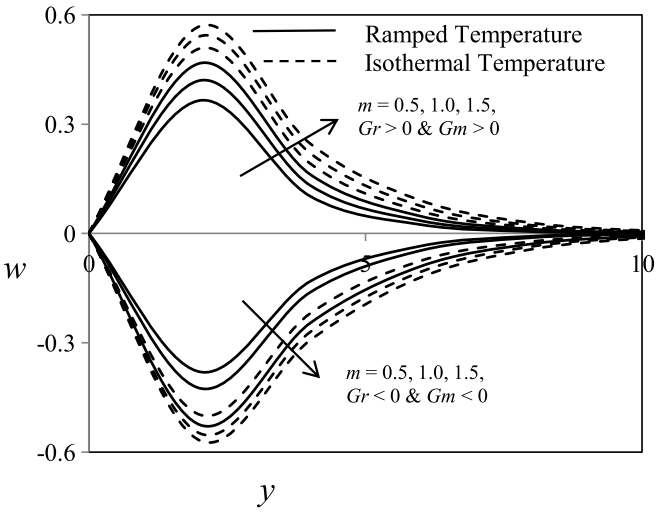

Fig. 6. Hall effect m on secondary velocity profiles.

increases in the entire region with an increase of hall current for ramped temperature and isothermal plates in case of cooling of the plate and the opposite effect in case of externally heating of the plate.

Figs. 7 and 8 show the effect of rotation on the primary and secondary velocity profiles for both ramped temperature and isothermal plate. The primary velocity exponentially decreases in the entire region where as the secondary velocity increases near to the plate and decreases away from the plate with increase of rotational parameter for ramped temperature and isothermal plate in case of cooling of the plate, the opposite effect in case of heating of the plate. Figs. 9 and 10 show the effect of Soret number on primary velocity and secondary velocity for both ramped temperature and isothermal plate. The primary and secondary velocity distribution exponentially increases in the entire region as an increase of Soret number for both ramped temperature and isothermal plate in case of cooling of the plate, and the opposite effect in case of heating of the plate. Figs. 11 and 12 show the effect of Dufour number on primary and secondary velocity distribution for both ramped temperature and isothermal plate. The primary and secondary velocity of the fluid exponentially increases in the entire region with an increase of Dufour number for both ramped temperature and isothermal plate in case of cooling of the plate, and the opposite effect in case of externally heating of the plate.

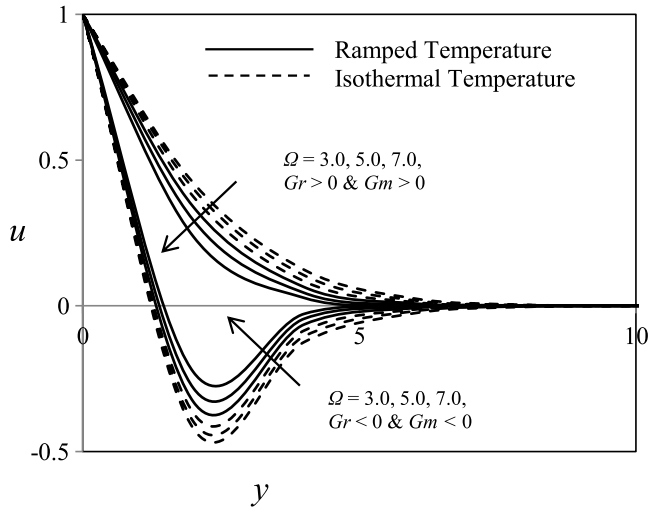

Fig. 7. Rotation effect Ω on primary velocity profiles.

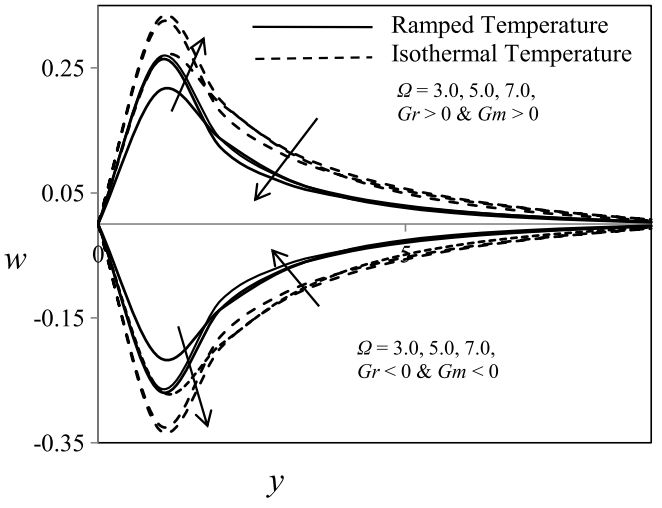

Fig. 8. Rotation effect Ω on secondary velocity profiles.

Tables 3–5 show variation of skin friction coefficient with the various values of Hall current, rotation parameter, Dufour and Soret number. The local skin friction coefficient due to primary velocity decreases with the increase in Hall current, Dufour and Soret number and decreases with increasing of rotation parameter. The local skin friction coefficient due to secondary velocity decreases with increasing of Dufour and Soret number while decreases with increasing of Hall current and rotation parameter for both ramped temperature and isothermal plate in case of cooling of the plate and the opposite effect in case of heating of the plate, it is observed from Tables 3–5.

6.2. *Temperature profiles*

Figs. 13(a), 13(b) show the effect of thermal radiation on temperature profiles with the absence and presence of Dufour number. The temperature increases in the entire boundary region with an increase of thermal radiation in the absence and presence of Dufour number for ramped temperature and isothermal plate. Figs. 14(a), Fig. 14(b) show the effect of Prandtl number on temperature profiles with the absence and presence of Dufour number. The temperature decreases in the entire boundary region with an increase of Prandtl number with the absence and presence of Dufour number for ramped temperature and isothermal plate. Fig. 15 shows the effect of Dufour number on temperature profiles, the temperature increases in the entire boundary region with an increase of Dufour number for both ramped

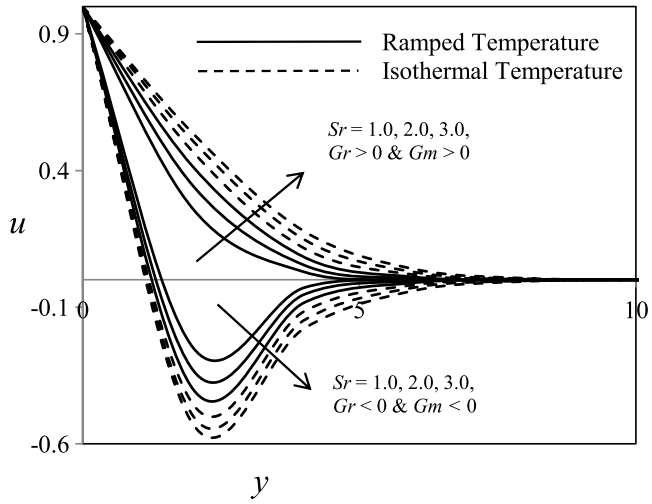

Fig. 9. Soret effect *Sr* on primary velocity profiles.

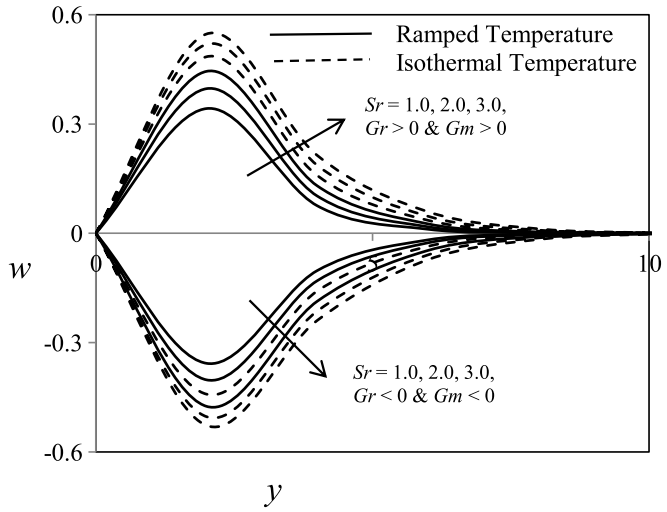

Fig. 10. Soret effect *Sr* on secondary velocity profiles.

Table 3
The skin-friction due to primary and secondary velocity with the effect of Dufour and Soret number in case of cooling and heating of the plate.

Dr	*Sr*	τ_x (cooling)		τ_z (cooling)		τ_x (heating)		τ_z (heating)	
		Ramped	Isothermal	Ramped	Isothermal	Ramped	Isothermal	Ramped	Isothermal
1	0	2.91033	2.35922	2.35311	2.63045	5.87581	6.42691	0.84429	0.56695
2	0	2.88051	2.32939	2.38692	2.66426	5.90564	6.45675	0.81048	0.53313
3	0	2.85066	2.29955	2.42074	2.69807	5.93547	6.48658	0.77667	0.49932
0	1	2.91676	2.36565	2.33259	2.62323	5.85768	6.42005	0.86481	0.57417
0	2	2.90506	2.34225	2.34589	2.64983	5.86938	6.44389	0.85151	0.54758
0	3	2.36565	2.31885	2.35918	2.67642	5.88109	6.46733	0.83822	0.52098

temperature and isothermal plate. Table 4 shows the variation of Nusselt number. The rate of heat transfer decreases with increase of thermal radiation and Dufour number and the opposite effect is observed for an increase of Prandtl number.

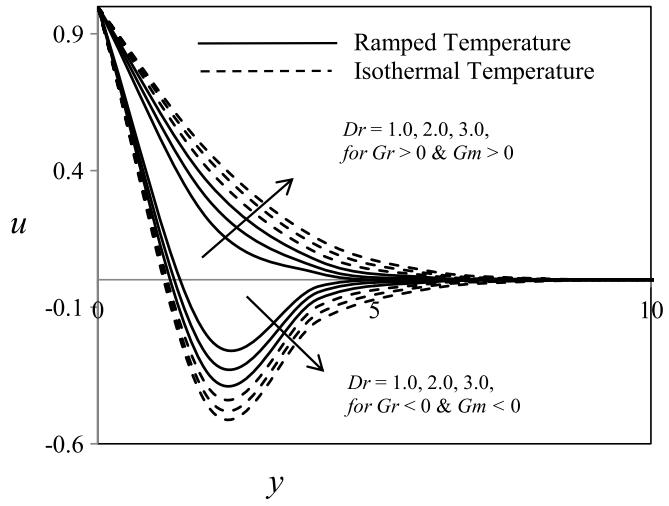

Fig. 11. Dufour effect *Dr* on primary velocity profiles.

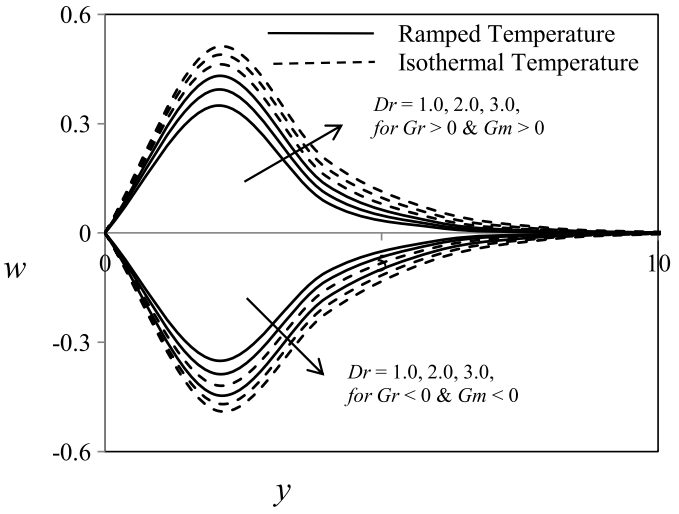

Fig. 12. Dufour effect *Dr* on secondary velocity profiles.

Table 4
The skin friction due to primary and secondary velocity with the effect of hall current and rotation in case of heating of the plate.

m	Ω	$-\tau_x$ (heating)		τ_z (heating)	
		Ramped	Isothermal	Ramped	Isothermal
0.5	5	−.5.8459	−6.39708	−0.8781	−0.60077
1	5	−5.6173	−6.17274	−0.1574	−0.80637
1.5	5	−5.3605	−5.93414	−1.2705	−0.87509
0.5	3	−5.7324	−6.33896	−1.6526	−0.41375
0.5	7	−6.0063	−6.50614	−1.0776	−0.77461

6.3. Concentration profiles

Fig. 16 shows the effect of Soret number on concentration field, the concentration profile increases in the entire region with an increase of Soret number. Figs. 17(a), 17(b) show the effect of Schmidt number on the concentration

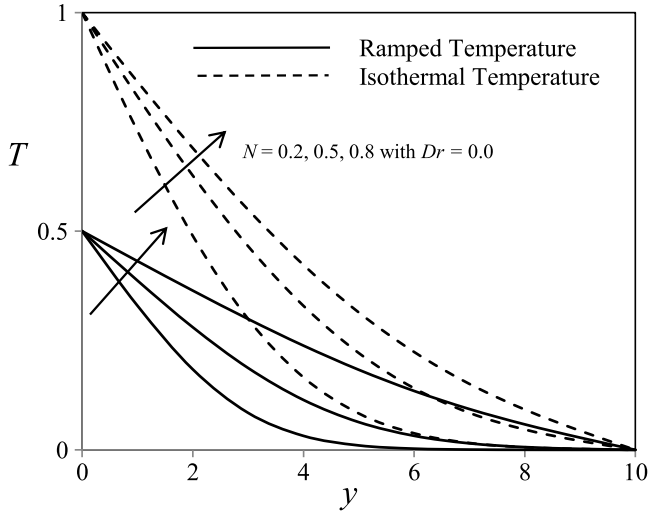

Fig. 13(a). Radiation effect N on temperature profiles with absence of Dufour.

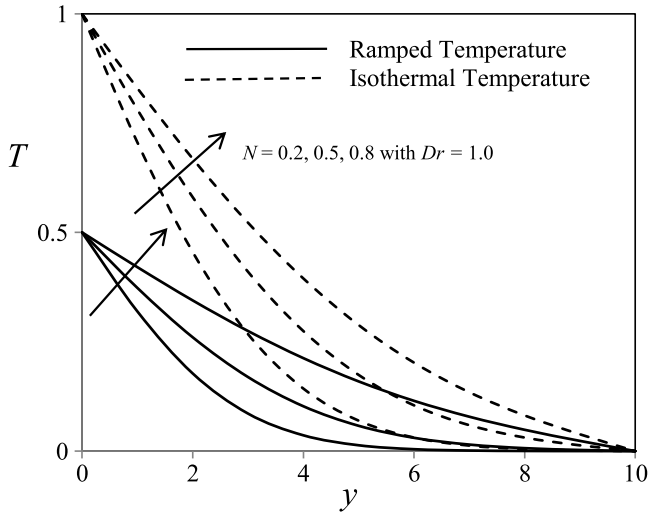

Fig. 13(b). Radiation effect N on temperature profiles with presence of Dufour.

Table 5
Rate of heat transfer near to the plate with the effect of radiation parameter, Prandtl number and Dufour number.

N	Pr	Dr	Nu	
			Ramped	Isothermal
0.2	0.71	0	0.17778	0.35556
0.5	0.71	0	0.16048	0.32096
0.2	0.71	1	0.83946	0.66168
0.5	0.71	1	0.67066	0.51018
5.0	0.71	0	0.12510	0.25021
5	7	0	0.24875	0.49752
5	0.71	1	0.04488	0.16999
5	7	1	0.61451	0.36577
5	0.71	2	0.19577	0.07068
5	0.71	3	0.35621	0.23110

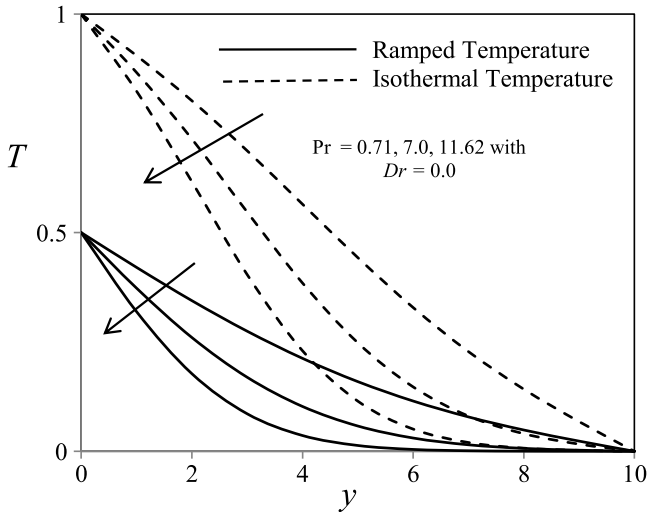

Fig. 14(a). Prandtl number *Pr* on temperature profiles with absence of Dufour.

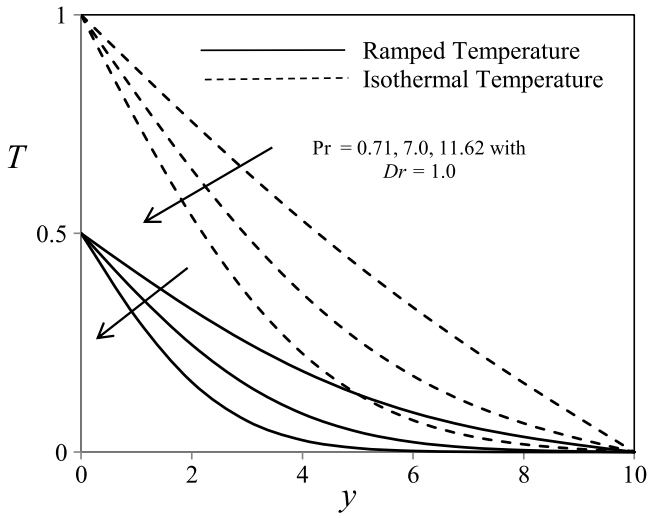

Fig. 14(b). Prandtl number *Pr* on temperature profiles with presence of Dufour.

profiles with the absence and presence of Soret number. The concentration linearly decreases for small values of Schmidt number and exponentially decreases for large values of Schmidt number in the entire boundary region in the absence of Soret number whereas exponentially decreases with increase of Schmidt number in the presence of Soret number. Table 6 shows that the rate of mass transfer increases with increasing of Schmidt number with the absence and presence of Soret number while decreases with an increase of Soret number.

7. Conclusions

The following conclusions are drawn from the above study, for both ramped temperature and isothermal plate.

1. The primary velocity increases with increasing of *Sr* and *Dr*, while decreases with increasing of M^2, m and Ω in case of cooling of the plate and opposite effects in case of heating of the plate.
2. The secondary velocity increases as increasing of m, *Sr* and *Dr* while decreases with increasing of M^2 and Ω in case of cooling of the plate and opposite effects in case of heating of the plate.
3. The temperature increases with increasing of N and the opposite effect for *Pr* while temperature increases with increasing of *Dr*.

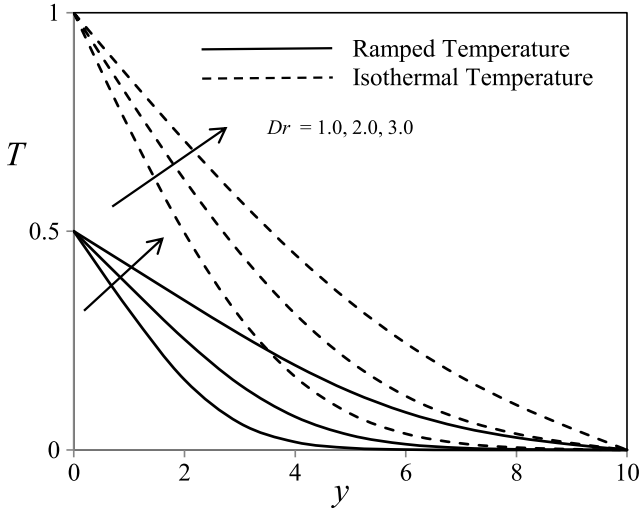

Fig. 15. Dufour effect *Dr* on temperature profiles.

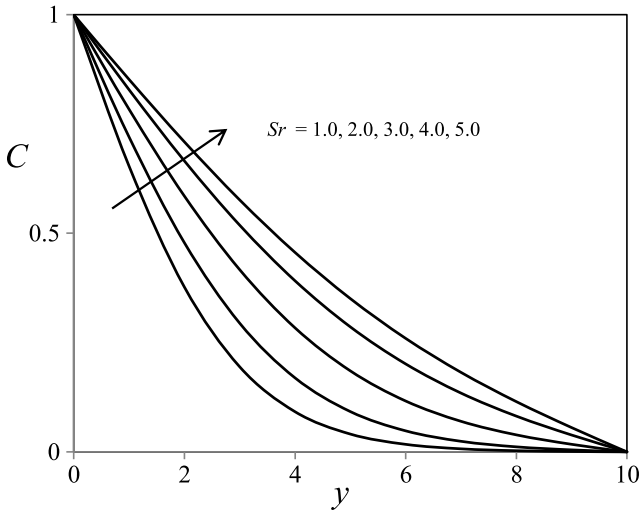

Fig. 16. Soret effect *Sr* on concentration profiles.

Table 6
Rate of mass transfer near to the plate with the effect of Schmidt number and Soret number.

Sc	*Sr*	*Sh*
0.22	0	0.49284
0.60	0	0.79023
0.22	1	0.25744
0.60	1	0.35794
0.22	2	0.20701
0.22	3	0.13156

4. Concentration profile decreases with increasing of *Sc* while increases with increasing of *Sr*.
5. Primary skin-friction coefficient increases with an increase of *Sr* and *Dr* while decreases with an increase of m and Ω in case of cooling of the plate and opposite effect for heating of the plate.

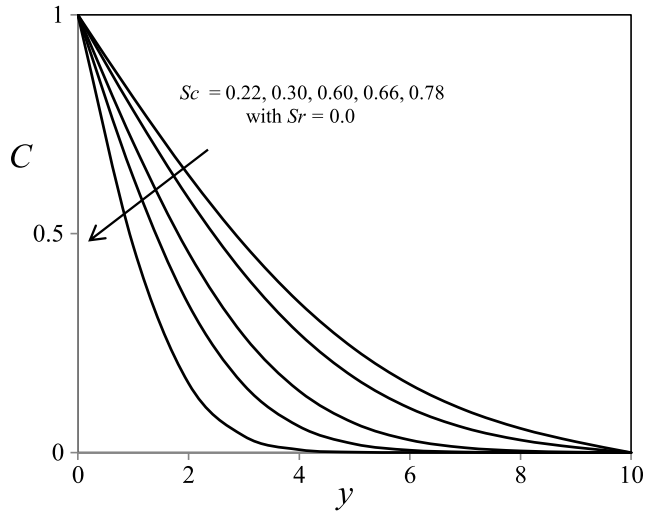

Fig. 17(a). Schmidt number *Sc* on concentration profiles with absence of Soret.

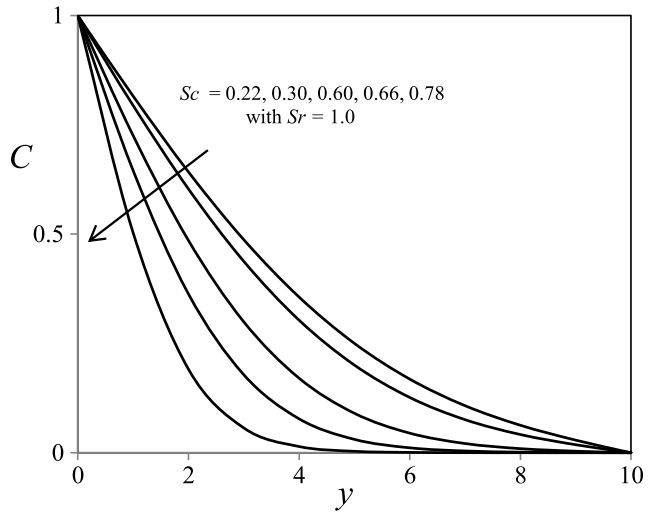

Fig. 17(b). Schmidt number *Sc* on concentration profiles with presence of Soret.

6. Secondary skin-friction coefficient increases with the increase of m, Ω, Dr and Sr in case of cooling of the plate and opposite effect in case of heating of the plate.
7. Heat transfer coefficient increases with increasing of Pr while decreases with increasing of N and Dr.
8. Mass transfer coefficient increases with increasing of Sc while decreases with increasing of Sr.
9. In case of cooling of the plate, the results of primary and secondary velocities and its skin-frictions are in good agreement with the results of Seth et al. [7] with the absence of Soret and Dufour.

Acknowledgments

The authors thank the reviewers for their constructive suggestions and comments, which have improved the quality of the article considerably. Also, the first and second authors are thankful to Dr. K. Tejaswani, GITAM University for her valuable suggestions, continuous support and encouragement in the preparation of this manuscript.

References

[1] Edwin Hall, On a new action of the magnet on electric currents, Amer. J. Math. 2 (1879) 287–292.
[2] Ajay Kumar Singh, N.P. Singh, Usha Singh, Hukum Singh, Convective flow past an accelerated porous plate in rotating system in presence of magnetic field, Int. J. Heat Mass Transfer 52 (2009) 3390–3395.
[3] I.U. Mbeledogu, A. Ogulu, Heat and mass transfer of an unsteady MHD natural convection flow of a rotating fluid past a vertical porous flat plate in the presence of radiative heat transfer, Int. J. Heat Mass Transfer 50 (2007) 1902–1908.
[4] J.G. Abuga, M. Kinyanjui, J.K. Sigey, An investigation of the effect of Hall currents and rotational parameter on dissipative fluid flow past a vertical semi-infinite plate, J. Eng. Tech. Res. 3 (2011) 314–320.
[5] N.C. Jain, H. Singh, Hall and thermal radiation effects on an unsteady rotating free convection slip flow along a porous vertical moving plate, Int. J. Appl. Mech. Eng. 17 (2012) 53–70.
[6] N. Ahmed, M. Dutta, Transient mass transfer flow past an impulsively started infinite vertical plate with ramped plate velocity and ramped temperature, Int. J. Physical Sci. 8 (2013) 254–263.
[7] G.S. Seth, S. Sarkar, S.M. Hussain, Effects of Hall current, radiation and rotation on natural convection heat and mass transfer flow past a moving vertical plate, Ain Shams Eng. 5 (2014) 489–503.
[8] A.J. Chamkha, M.A. Mansour, A. Aly, Unsteady MHD free convective heat and mass transfer from a vertical porous plate with Hall current, thermal radiation and chemical reaction effects, Internat. J. Numer. Methods Fluids (2009). http://dx.doi.org/10.1002/fld.2190.
[9] S. Sivaiah, R. Srinivasa Raju, Finite element solution of heat and mass transfer flow with hall current, heat source and viscous dissipation, Appl. Math. Mech. 34 (2013) 559–570.
[10] Siva Reddy Sheri, R. Srinivasa Raju, Transient MHD free convective flow past an infinite vertical plate embedded in a porous medium with viscous dissipation, Meccanica (2015). http://dx.doi.org/10.1007/s11012-015-0285-y.
[11] J. Anand Rao, R. Srinivasa Raju, S. Sivaiah, Finite Element Solution of MHD transient flow past an impulsively started infinite horizontal porous plate in a rotating fluid with Hall current, J. Appl. Fluid Mech. 5 (2012) 105–112.
[12] J. Anand Rao, R. Srinivasa Raju, S. Sivaiah, Finite Element Solution of heat and mass transfer in MHD Flow of a viscous fluid past a vertical plate under oscillatory suction velocity, J. Appl. Fluid Mech. 5 (2012) 1–10.
[13] M.V. Ramana Murthy, R. Srinivasa Raju, J. Anand Rao, Heat and Mass transfer effects on MHD natural convective flow past an infinite vertical porous plate with thermal radiation and Hall Current, Procedia Eng. J. 127 (2015) 1330–1337.
[14] G. Jithender Reddy, J.A. Rao, R. Srinivasa Raju, Chemical reaction and radiation effects on MHD free convection from an impulsively started infinite vertical plate with viscous dissipation, Int. J. Adv. Appl. Math. Mech. 2 (3) (2015) 164–176.
[15] J. Anand Rao, G. Jithender Reddy, R. Srinivasa Raju, Finite element study of an unsteady MHD free convection Couette flow with viscous Dissipation, Glob. J. Pure Appl. Math. 11 (2) (2015) 65–69.
[16] R. Srinivasa Raju, G. Jithender Reddy, J. Anand Rao, P. Manideep, Application of FEM to free convective flow of Water near 4 °C past a vertical moving plate embedded in porous medium in presence of magnetic field, Glob. J. Pure Appl. Math. 11 (2) (2015) 130–134.
[17] M. Sheikholeslami, M.M. Rashidi, Effect of space dependent magnetic field on free convection of Fe3O4-water nanofluid, J. Taiwan Inst. Chem. Eng. 56 (2015) 6–15.
[18] M. Sheikholeslami, M.M. Rashidi, Ferrofluid heat transfer treatment in the presence of variable magnetic field, Eur. Phys. J. Plus 130 (2015) 115.
[19] M.M. Rashidi, Mohammad Nasiri, Marzieh Khezerloo, Najib laraqi numerical investigation of magnetic field effect on mixed convection heat transfer of nanofluid in a channel with sinusoidal walls, J. Magn. Magn. Mater. 401 (2016) 159–168.
[20] M.M. Rashidi, E. Erfani, Analytical method for solving steady MHD convective and slip flow due to a rotating disk with viscous dissipation and ohmic heating, Eng. Comput. 29 (6) (2012) 562–579.
[21] M.S. Alam, M.M. Rahman, Dufour and soret effects on mixed convection flow past a vertical porous flat plate with variable suction, Nonlinear Anal. Model. Control 11 (2006) 3–12.
[22] H.A.M. El-Arabawy, Soret and dufour effects on natural convection flow past a vertical surface in a porous medium with variable surface temperature, J. Math. Stat. 5 (2009) 190–198.
[23] N.G. Kafoussias, E.W. Williams, Thermal-diffusion and diffusion-thermo effects on mixed free-forced convective and mass transfer boundary layer flow with temperature dependent viscosity, Internat. J. Engrg. Sci. 33 (1995) 1369–1384.
[24] Nabil Eldabe, Mahmoud Abu Zeid, Thermal Diffusion and Diffusion Thermo effects on the viscous fluid flow with heat and mass transfer through porous medium over a shrinking sheet, J. Appl. Math. 2013 (2013).
[25] S. Srinivas, A. Subramanyam Reddy, T.R. Ramamohan, Anant Kant Shukla, Thermal-diffusion and diffusion-thermo effects on MHD flow of viscous fluid between expanding or contracting rotating porous disks with viscous dissipation, J. Egyptian Math. Soc. 24 (1) (2016) 101–107.
[26] D. Srinivasacharya, Ch. RamReddy, Soret and Dufour effects on mixed convection from an exponentially stretching surface, Int. J. Nonlinear Sci. 12 (2011) 60–68.
[27] D. Srinivasacharya, Ch. Ram Reddy, J. Pranitha, A. Postelnicu, Soret and dufour effects on non-darcy free convection in a power-law fluid in the presence of magnetic field and stratification, Heat Transfer-Asian Res. 43 (2014) 592–606.
[28] D. Srinivasacharya, B. Mallikarjuna, R. Bhuvanavijaya, Soret and dufour effects on mixed convection along a wavy surface in a porous medium with variable properties, Ain Shams Eng. J. 6 (2015) 553–564.
[29] Ch. RamReddy, P.V.S.N. Murthy, A.J. Chamkha, A.M. Rashad, Soret effect on mixed convection flow in a nanofluid under convective boundary condition, Int. J. Heat Mass Transfer 64 (2013) 384–392.
[30] G. Jithender Reddy, R. Srinivasa Raju, Siva Reddy Sheri, Finite element analysis of soret and radiation effects on transient mhd free convection from an impulsively started infinite vertical plate with heat absorption, Int. J. Math. Arch. 5 (2014) 211–220.
[31] A.K. Ahmed, P. Sibanda, On A linearization method for MHD flow past a rotating disk in porous medium with cross-diffusion and hall effects, J. Porous Media 16 (2013) 1011–1024.

[32] R. Srinivasa Raju, Combined influence of thermal diffusion and diffusion thermo on unsteady hydromagnetic free convective fluid flow past an infinite vertical porous plate in presence of chemical reaction, J. Inst. Eng. (India): Series C (2016) 1–11. http://dx.doi.org/10.1007/s40032-016-0258-5.
[33] R. Srinivasa Raju, B. Mahesh Reddy, M.M. Rashidi, R.S.R. Gorla, Application of finite element method to unsteady mhd free convection flow past a vertically inclined porous plate including thermal diffusion and diffusion thermo effects, J. Porous Media (2016) in press.
[34] R. Srinivasa Raju, K. Sudhakar, M. Rangamma, The effects of thermal radiation and Heat source on an unsteady MHD free convection flow past an infinite vertical plate with thermal-diffusion and diffusion-thermo, J. Inst. Eng. (India): Series C 94 (2013) 175–186.
[35] Siva Reddy Sheri, R. Srinivasa Raju, Soret effect on unsteady MHD free convective flow past a semi-infinite vertical plate in the presence viscous dissipation, Int. J. Comput. Methods Eng. Sci. Mech. 1 (6) (2015) 132–141.
[36] M.A. Abdelraheem, M.A. Mansour, A.J. Chamkha, Effects of soret and dufour numbers on free convection over isothermal and adiabatic stretching surfaces embedded in porous media, J. Porous Media 14 (2011) 67–72.
[37] A.K. Ahmed, P. Sibanda, Effect of temperature-dependent viscosity on MHD mixed convective flow from an exponentially stretching surface in porous media with cross-diffusion, Spec. Top. Rev. Porous Media: Int. J. 5 (2014) 157–170.
[38] K.R. Cramer, S.I. Pai, Magneto Fluid Dynamics for Engineers and Applied Physicists, McGraw Hill Book Company, NY, 1973.
[39] E.M. Sparrow, R.D. Cess, Radiation Heat Transfer, Brooks/Cole, Belmont, Calif., 1966.
[40] T. Belytschko, Y.Y. Lu, L. Gu, Element free Galerkin method, Internat. J. Numer. Methods Engrg. 37 (1994) 229–256.
[41] W.K. Liu, S. Jun, Y.F. Zhang, Reproducing Kernel particle Method, Internat. J. Numer. Methods Engrg. 20 (1995) 1081–1106.
[42] E.S. Onate, O.C. Idelsohn, R.L. Zienkiewicz, Taylors, A finite point method in computational mechanics. Application to convective transport and fluid flow, Internat. J. Numer. Methods Engrg. 39 (12) (1996) 3839–3967.
[43] C.A. Duarte, J.T. Oden, H-p clouds an h-p meshless method, Numer. Methods Partial Differential Equations (1996) 1–34.
[44] T. Belytschko, Y. Kroangauz, M. Fleming, D. Organ, W.K. Lui, Meshless Methods: An overview and recent developments, Comput. Methods Appl. Mech. Eng. 139 (1996) 3–47.
[45] Rajesh Sharma, R. Bhargava, Peeyush Bhargava, A numerical solution of unsteady MHD convection heat and mass transfer past a semi-infinite vertical porous moving plate using element free Galerkin method, Comput. Mater. Sci. 48 (3) (2010) 537–543.
[46] Ryszard Staroszczyk, Application of an element-free Galerkin method to water wave propagation problems, Arch. Hydro Eng. Environ. Mech. 60 (2014) 87–105.
[47] Sonam Singh, Rama Bhargava, Numerical simulation of a phase transition problem with natural convection using hybrid FEM/EFGM technique, Internat. J. Numer. Methods Heat Fluid Flow 25 (3) (2015) 570–592.
[48] Rajesh Sharma, R. Bhargav, Numerical simulation of MHD Hiemenz flow of a micropolar fluid towards a nonlinear stretching surface through a porous medium, Int. J. Comput. Methods Eng. Sci. Mech. 16 (4) (2015) 234–245.
[49] R. Srinivasa Raju, G. Jithender Reddy, J. Anand Rao, M.M. Rashidi, Rama Subba Reddy Gorla, Analytical and numerical study of unsteady MHD free convection flow over an exponentially moving vertical plate with heat absorption, Int. J. Therm. Sci. 107 (2016) 303–315.
[50] A. Singh, I.V. Singh, R. Prakash, Numerical analysis of fluid squeezed between two parallel plates by meshless method, Comput. & Fluids 36 (2007) 1460–1480.
[51] I.V. Singh, A numerical solution of composite heat transfer problems using meshless method, Int. J. Heat Mass Transfer 47 (2004) 2123–2138.
[52] T. Zhu, S.N. Atluri, A modified collocation method and a penalty formulation for enforcing the essential boundary conditions in the element free galerkin method, Comput. Mech. 21 (1998) 211–222.
[53] G.D. Smith, Numerical Solutions of Partial Differential Equations-Finite Difference Methods, third ed., Oxford University Press, New York, 1985.
[54] C.Y. Warner, V.S. Arpaci, An experimental investigation of turbulent natural convection in air at low pressure along a vertical heated flat plat, Int. J. Heat Mass Transfer 11 (1968) 397–406.